Electronic Supplementary Information

Experimental section

Preparation of materials: The medium-entropy tunnel-type (T-type) $Na_{0.44}MnO_2$ samples were synthesized by a simple solid-state reaction method. Stoichiometric Na_2CO_3 (5 wt% excess to compensate for sodium evaporation), $MnCO_3$, $Al(OH)_3$, TiO_2, and CoO were balled in ethanol for half six hours. Then the obtained precursors were sintered at 900 °C for 12 h under the air atmosphere in a muffle furnace. In comparison, the T-type $Na_{0.44}MnO_2$ materials were synthesized by a similar route without adding Al and Ti and Co sources. For convenience, $Na_{0.44}MnO_2$, $Na_{0.44}Mn_{0.97}Al_{0.01}Ti_{0.01}Co_{0.01}O_2$, $Na_{0.44}Mn_{0.94}Al_{0.02}Ti_{0.02}Co_{0.02}O_2$, $Na_{0.44}Mn_{0.91}Al_{0.03}Ti_{0.03}Co_{0.03}O_2$ are referred as NMO, NMO-1, NMO-2, and NMO-3, respectively.

Materials Characterization: The structures of the samples were measured by X-ray diffraction (XRD) on a Philips X' Pert Super diffractometer with Cu Kα (λ=1.54182 Å), The morphologies of the samples were characterized on scanning electron microscopy (SEM, JEOL-JSM-6700F), transmission electron microscopy (TEM, Hitachi H7650) and high-resolution transmission electron microscopy (HR-TEM, JEM-2100F) with an energy-dispersive X-ray spectrometer (EDX). X-ray photoelectron spectroscopy (XPS) was collected on an ESCALAB 250 X-ray photoelectron spectrometer (Perkin-Elmer) was occupied to perform the distribution of elements on the surface of materials. Inductively coupled plasma optical emission spectroscopy was used to estimate the Na/M (M = Mn, Al, Ti, Co) ratios in materials (ICP-OES).

Electrochemical measurement: Using N-methyl-2-pyrrolidone (NMP) as a solvent, Previously. The electrodes had been prepared by mixing 70 wt % active materials, 20 wt % Super P, and 10 wt %polyvinylidene fluoride (PVDF) binder to form a slurry, which was then coated on aluminum foil. The aluminum foil was then dried overnight in a vacuum oven at 100 °C for 12 h. Following that, the working electrodes were removed and pressed at a pressure of 20 MPa. The electrolyte used was 1.0 mol L^{-1} $NaClO_4$ in an ethylene carbonate (EC)−diethyl carbonate (DEC) solution (1:1 v/v) with 5 vol % of fluoroethylene carbonate (FEC), and glass fiber membrane (Whatman, GF/D) as separator were assembled to form 2032-coin cells. Sodium foil was cut from a sodium bulk stored in mineral oil and used as the counter electrode. In an argon-filled glove box, the cells were assembled. The galvanostatic cycling test was measured by the Land CT2001A battery test system between 2.0 and 4.0 V at 25 °C. Using a CHI 660b electrochemistry workstation between 4.0 and 2.0 V, cyclic voltammetry (CV) at a scan rate of 0.1 to 1 mV s^{-1} and electrochemical impedance spectroscopy (EIS) from 100 kHz to 100 MHz were performed. The diffusion coefficient of Na^+ was studied using the galvanostatic intermittent titration technique (GITT) and EIS. For the GITT measurement, the cells were charged and discharged at 0.1 C for 300 s followed by open-circuit relaxation for 1 h. The procedure was maintained until the voltage reached 4.0 or 2.0 V.

Theoretical Calculations: Spin-polarized calculations are performed in the framework of the density functional theory (DFT) with the projector augmented plane-wave method, as implemented in the Vienna ab initio simulation package. The generalzied gradient approximation proposed by Perdew, Burke, and Ernzerhof is selected for the exchange-correlation potential.. The effects due to the localization of the d-orbital electrons of TM-ions were taken into account with the GGA + U approach. The effective U values were set to 3.9 eV Ru. The cut-off energy for plane wave is set to 520 eV. The energy criterion is set to 10^{-6} eV in iterative solution of the Kohn-Sham equation. The Gamma k-point mesh was sampled with a separation of about 0.03 $Å^{-1}$ in the Brillouin zone. All the structures are relaxed until the residual forces on the atoms have declined to less than 0.03 eV/Å.

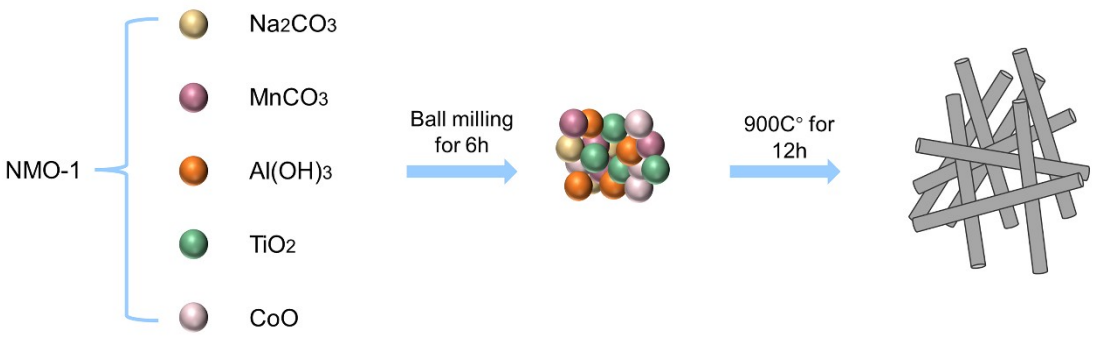

Figure S1: Preparation method of NMO-1.

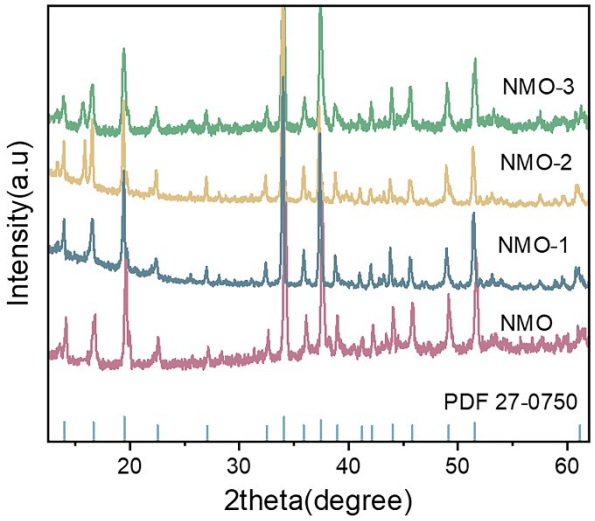

Figure S2: XRD patterns of $Na_{0.44}MnO_2$ (NMO), $Na_{0.44}Mn_{0.97}(Al,Ti,Co)_{0.01}O_2$ (NMO-1), $Na_{0.44}Mn_{0.94}(Al,Ti,Co)_{0.02}O_2$ (NMO-2), $Na_{0.44}Mn_{0.91}(Al,Ti,Co)_{0.03}O_2$ (NMO-3).

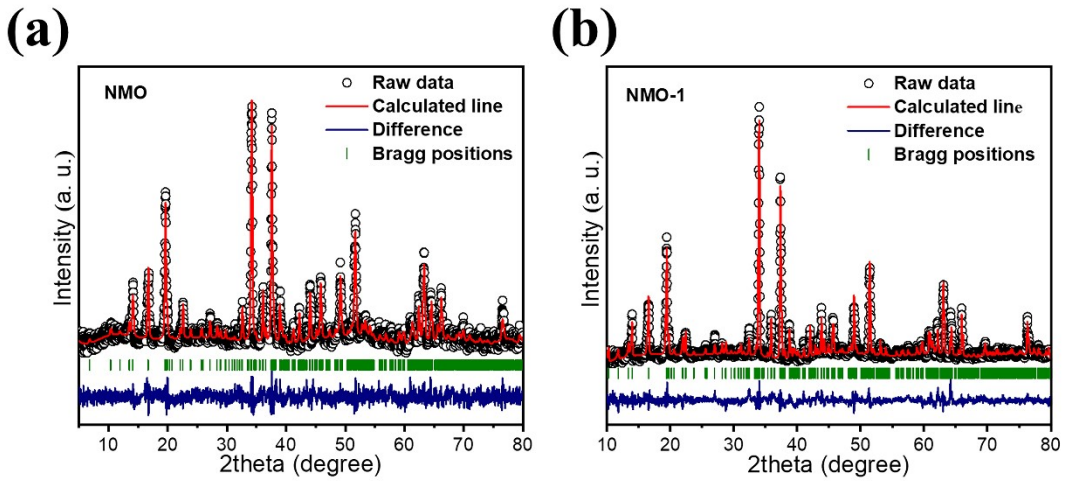

Figure S3: (a) Rietveld refinement of the NMO, (b) and NMO-1.

Samples	a, Å	b, Å	c, Å	V, Å^3	Rwp, %	Rp, %
NMO	9.09440	26.38520	2.82563	676.2	3.55	2.8
NMO-1	9.11232	26.39303	2.83030	680.6	1.13	0.82

Table S1: The lattice parameters of T-type phases obtained from Rietveld refinement of NMO, NMO-1 samples.

Space group: Pbam					
atom	x	y	z	Wyckoff	Occupancy
Na1	0.1674	0.2231	0.0000	4g	1
Na2	0.1895	0.4183	0.5000	4h	1
Na3	0.1477	0.0185	0.0000	4g	1
Mn1	0.0312	0.3061	0.0000	4g	1
Mn2	0.3541	0.0894	0.5000	4h	1
Mn3	0.0000	0.5000	0.0000	2c	1
Mn4	0.3766	0.3063	0.5000	4h	1
Mn5	0.0296	0.1139	0.0000	4g	1
O1	0.3471	0.0040	0.5000	4h	1
O2	0.1711	0.0657	0.0000	4g	1
O3	0.0041	0.1518	0.5000	4h	1
O4	0.4572	0.1925	0.5000	4h	1
O5	0.2357	0.2780	0.5000	4h	1
O6	0.2635	0.3539	0.0000	4g	1
O7	0.2773	0.4018	0.0000	4g	1
O8	0.5048	0.0674	0.0000	4g	1
O9	0.4946	0.4467	0.5000	4h	1

Table S2: Crystallographic parameters of $Na_{0.44}MnO_2$ refined by Rietveld method.

Space group: Pbam					
atom	x	y	z	Wyckoff	Occupancy
Na1	0.2024	0.1997	0.0000	4g	1
Na2	0.2033	0.4021	0.5000	4h	1
Na3	0.1644	0.0246	0.0000	4g	1
Mn1	0.0357	0.3067	0.0000	4g	0.999
Mn2	0.3565	0.0920	0.5000	4h	0.990
Mn3	0.0000	0.5000	0.0000	2c	0.997
Mn4	0.3694	0.3033	0.5000	4h	0.994
Mn5	0.0104	0.1107	0.0000	4g	0.990
O1	0.3311	0.0015	0.5000	4h	1
O2	0.2424	0.1062	0.0000	4g	1
O3	0.1000	0.1810	0.5000	4h	1
O4	0.4350	0.1843	0.5000	4h	1
O5	0.1436	0.2882	0.5000	4h	1
O6	0.2949	0.2442	0.0000	4g	1
O7	0.3394	0.3638	0.0000	4g	1
O8	0.5324	0.0748	0.0000	4g	1
O9	0.5038	0.4442	0.5000	4h	1
Al2	0.3565	0.0920	0.0000	4h	0.006
Al5	0.0104	0.1107	0.0000	4g	0.004
Ti1	0.0357	0.3067	0.0000	4g	0.001
Ti3	0.000	0.5000	0.0000	2c	0.003
Ti4	0.3694	0.3633	0.5000	4h	0.006
Co2	0.3565	0.0920	0.5000	4g	0.004
Co5	0.0104	0.1107	0.0000	4g	0.006

Table S3: Crystallographic parameters of NMO-1 refined by Rietveld method.

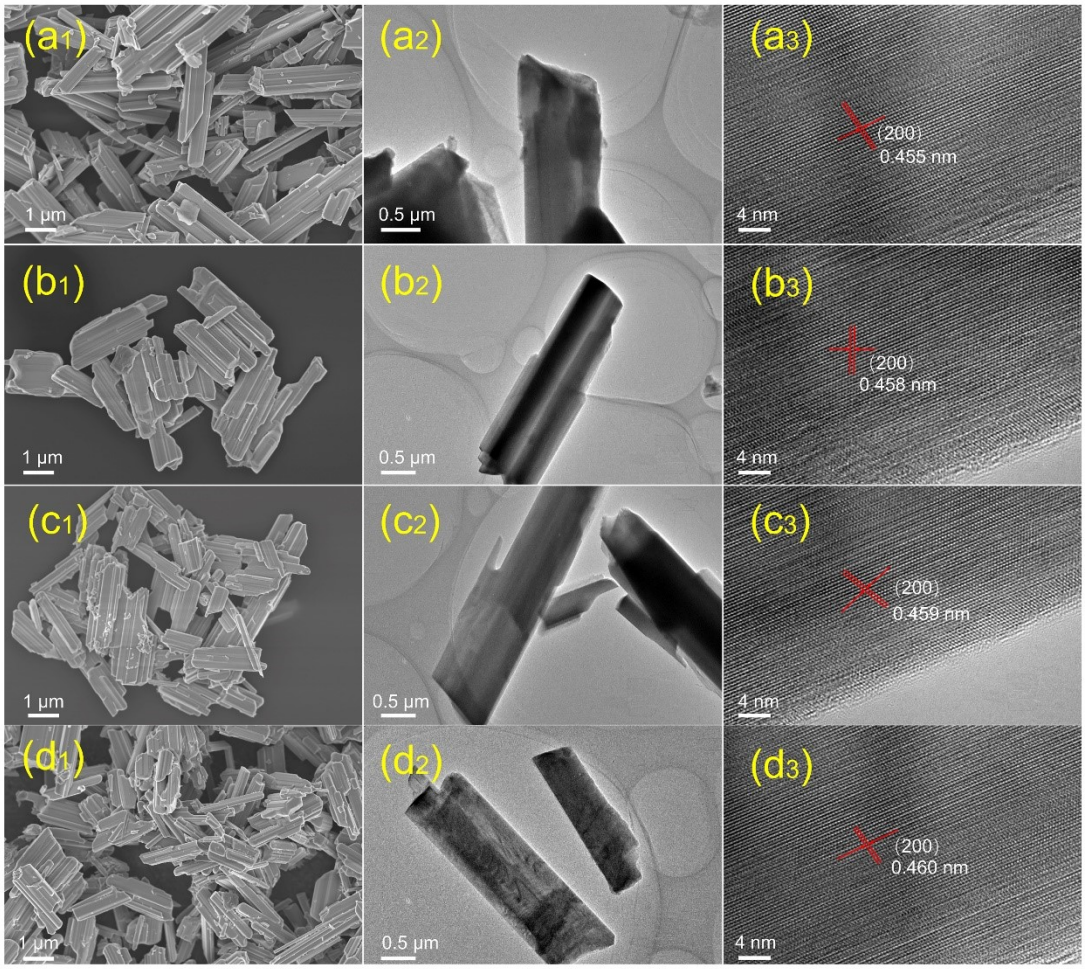

Figure S4: (a_1, a_2, a_3),SEM, TEM and HR-TEM images of NMO, (b_1, b_2, b_3) NMO-1, (c_1, c_2, c_3) NMO-2, (d_1, d_2, d_3) and NMO-3.

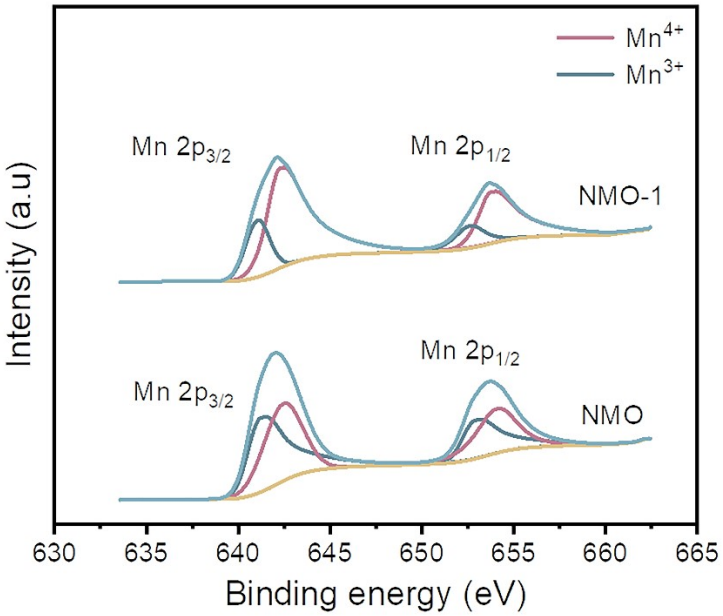

Figure S5: XPS patterns of Mn 2p in NMO and NMO-1 samples, respectively.

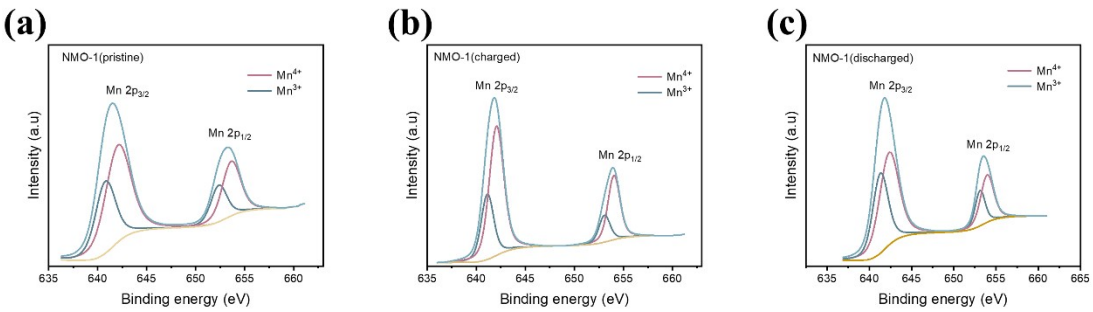

Figure S6: Ex situ XPS spectra of NMO-1 during initial charge and discharge at a current rate of 0.1 C between 2.0 and 4.0 V voltage range.

Samples	Na	Mn
charged	0.202	0.997
discharged	0.682	0.997

Table S4: The atomic ratios of Na/Mn the fully charged NMO-1 and discharged sample determined by ICP-OES (regard M=1).

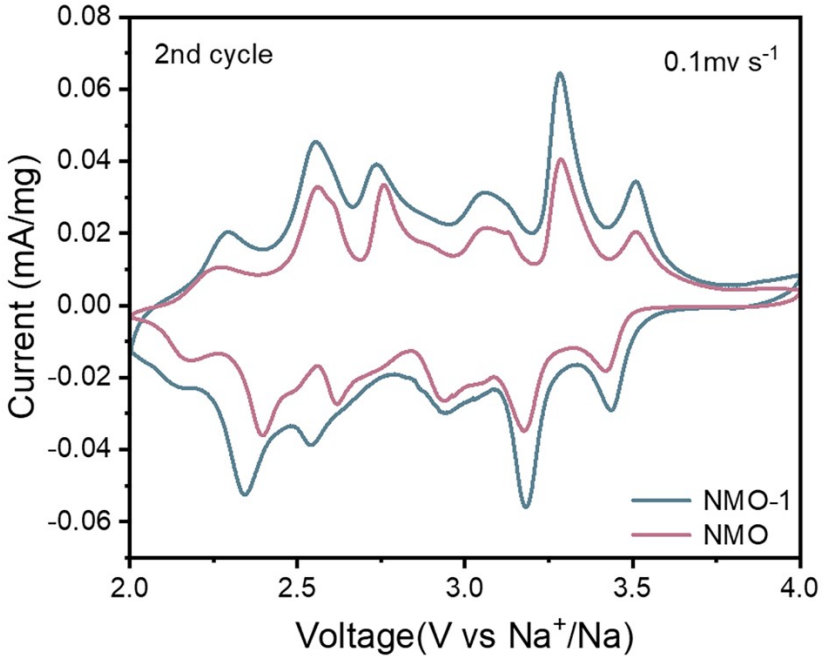

Figure S7: The 2nd cycle CV curves of NMO and NMO-1 at 0.1 mv s^{-1}.

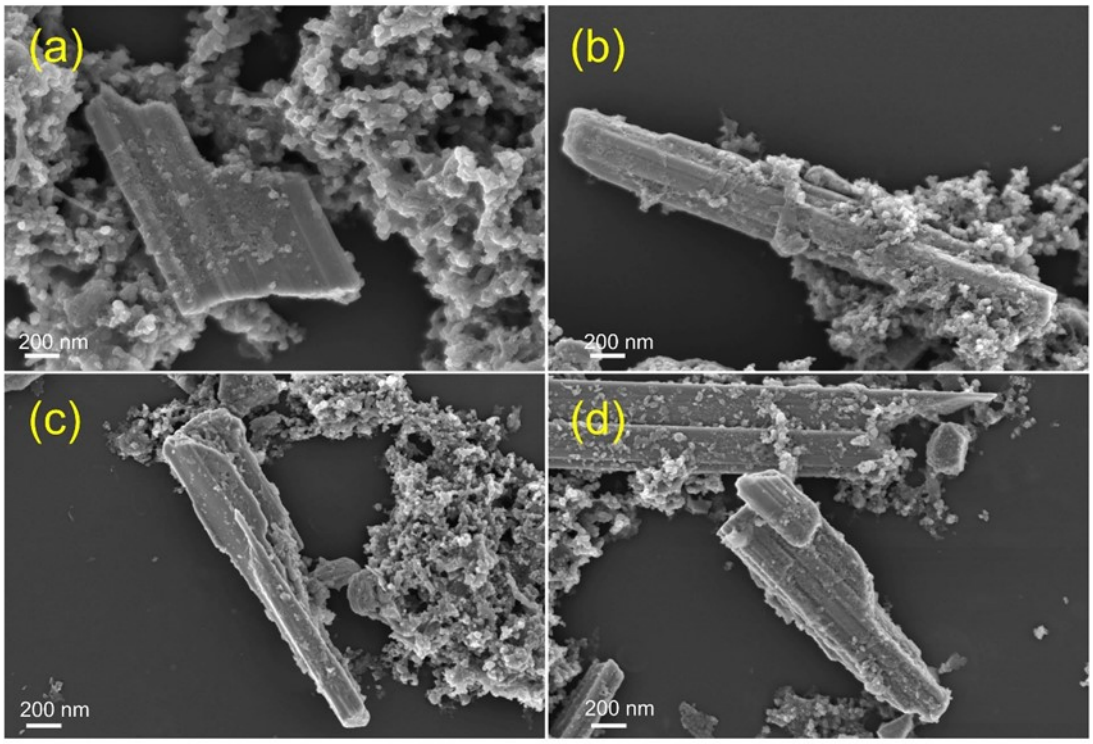

Figure S8: (a) SEM images of NMO, (b) NMO-1, (c) NMO-2, (d) and NMO-3 after 2000 cycles at the current rate of 10 C.

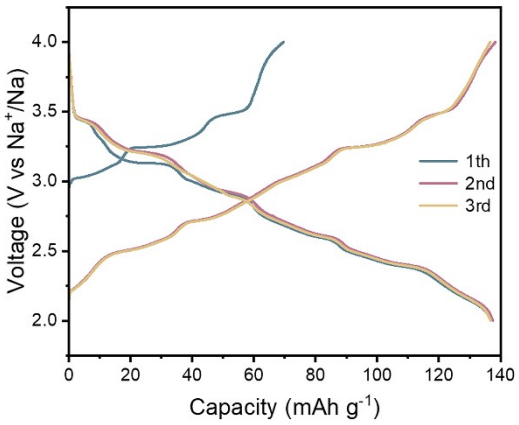

Figure S9: The charge-discharge profile of initial three cycles of NMO-1 electrode at 0.1 C.

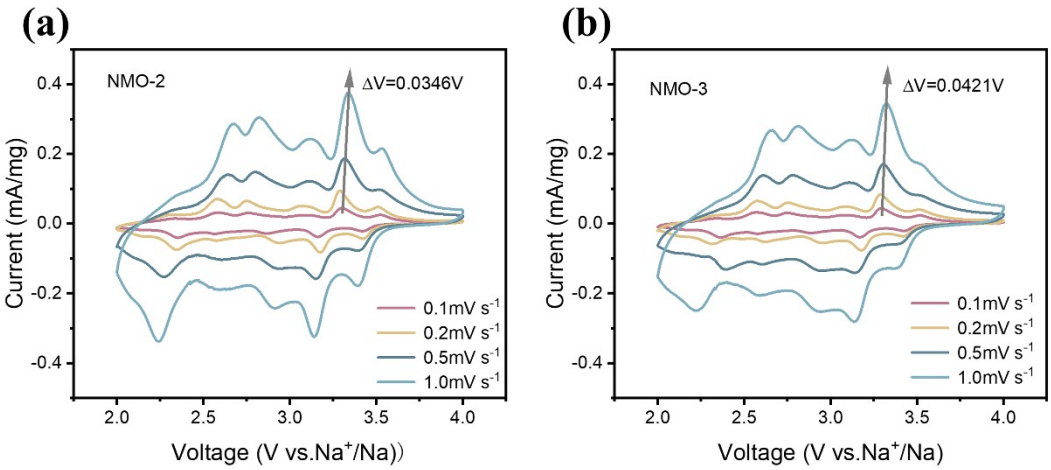

Figure S10: (a) CV curves of the NMO-2, (b) and NMO-3 at the different scanning rates increasing from 0.1 to 1.0 mv s^{-1}.

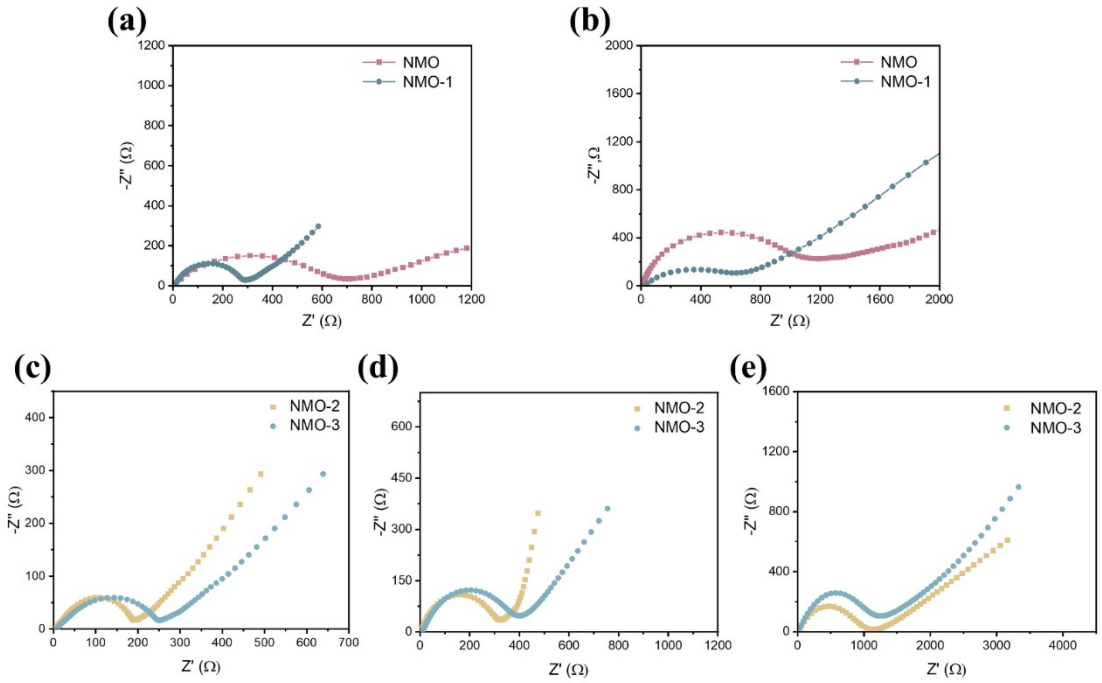

Figure S11: (a) Nyquist plot of NMO and NMO-1 after 100 cycles at 10C, (b) and Nyquist plot of NMO and NMO-1 after 1000 cycles at 10C. (c) Nyquist plots of NMO-2 and NMO-3 before cycling, (d) and nyquist plot of NMO-2 and NMO-3 after 100 cycles at 10C. (e) Nyquist plot of NMO-2 and NMO-3 after 1000 cycles at 10C.

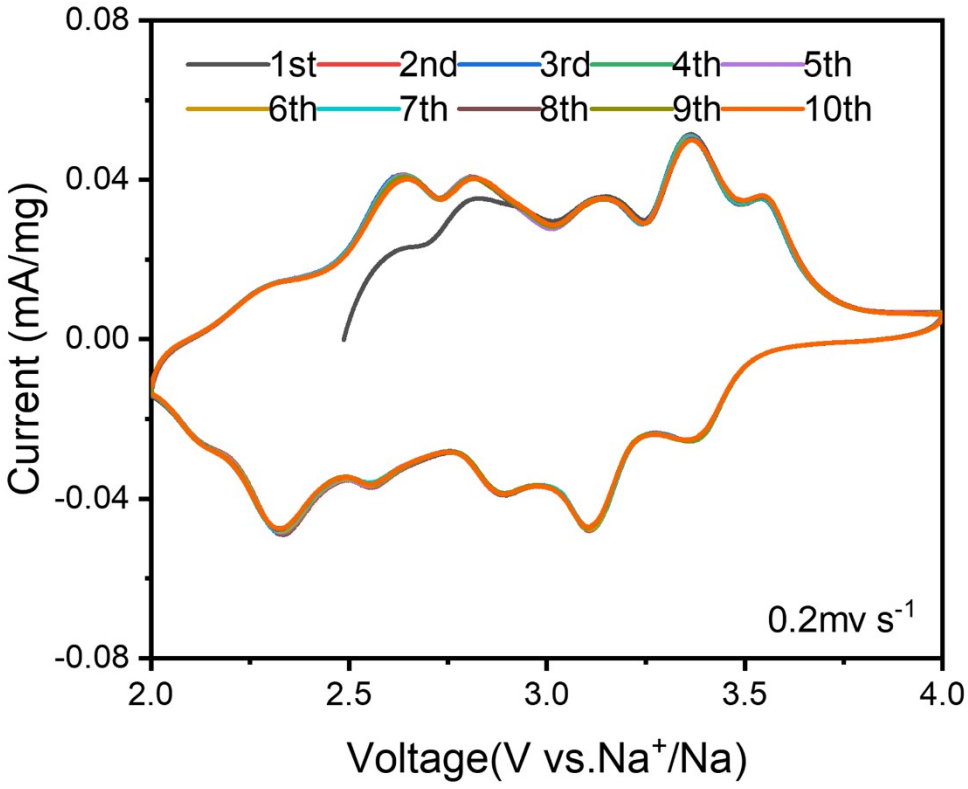

Figure S12: CV curves of NMO-1 at a scan rate of 0.2 mV s^{-1}.

Samples	Before cycling		After 100 cycles		After 1000 cycles	
	Rs, Ω	Rct, Ω	Rs, Ω	Rct, Ω	Rs, Ω	Rct, Ω
NMO	5.912	464.9	6.424	782.4	12.396	1264,9
NMO-1	4.632	157.8	5.301	274.8	6.132	701.8
NMO-2	4.783	193.4	5.678	315.6	10.565	1116.4
NMO-3	4.921	247.1	5.902	400.8	11.382	1235.7

Table S5: Impedance parameters derived using equivalent circuit model for NMO, NMO-1, NMO-2 and NMO-3 before cycling and after cycling.

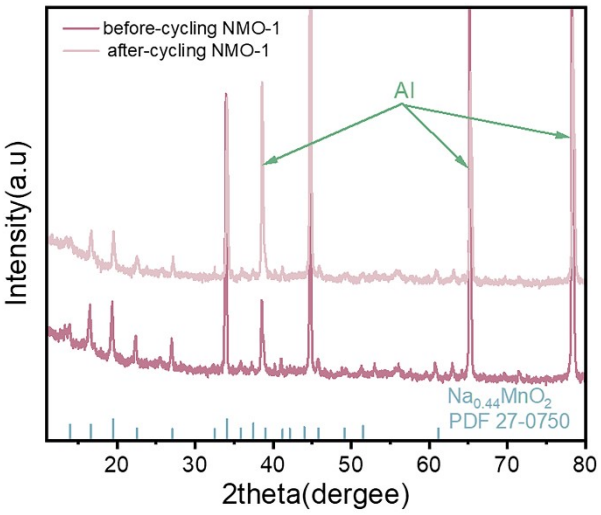

Figure S13: The XRD patterns of NMO-1 before and after cycling.

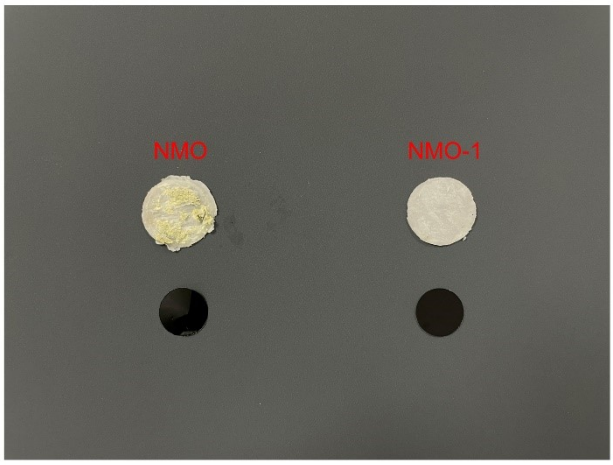

Figure S14: The picture of diaphragms and pole pieces after 1000 cycles for pristine NMO and NMO-1.

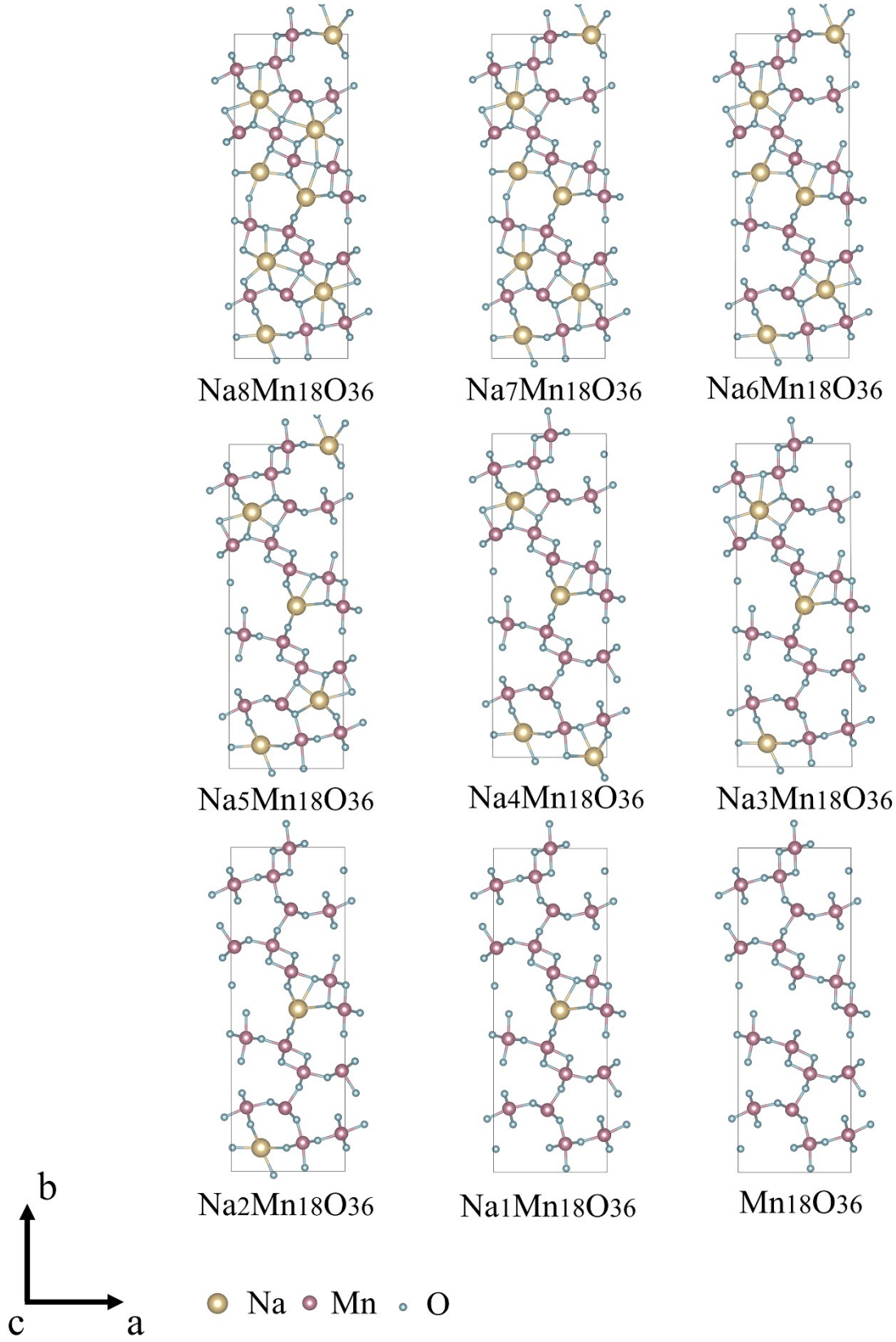

Figure S15: $Na_8Mn_{18}O_{36}$ Structure Evolution Diagram of Na^+ intercalation and extraction.

	a (Å)	b (Å)	c (Å)	Volume (Å^3)
$Na_8Mn_{18}O_{36}$	9.22585	26.36779	2.91262	708.539925
$Na_7Mn_{18}O_{36}$	9.18141	26.20375	2.91181	700.544852
$Na_6Mn_{18}O_{36}$	9.14358	26.03411	2.90665	691.913242
$Na_5Mn_{18}O_{36}$	9.12525	25.94757	2.90438	687.694691
$Na_4Mn_{18}O_{36}$	9.10057	25.75171	2.90677	681.215968
$Na_3Mn_{18}O_{36}$	9.08100	25.67574	2.90870	678.183335
$Na_2Mn_{18}O_{36}$	9.02618	25.70514	2.90858	674.845777
$Na_1Mn_{18}O_{36}$	8.97875	25.64249	2.90839	669.523713
$Mn_{18}O36$	8.95734	25.67677	2.90839	668.918203

Table S6: The shifting lattice parameters of $Na_{0.44}MnO_2$ obtained from DFT.

Elements	NMO	NMO-1	NMO-2	NMO-3
Na	0.4394	0.4402	0.4412	0.4408
Mn	1.0000	0.9703	0.9412	0.9109
Al	-	0.0101	0.0197	0.0302
Ti	-	0.0100	0.0203	0.0304
Co	-	0.0102	0.0210	0.0303

Table S7: The atomic ratios of Na/M (M = Mn, Al,Ti,Co) in NMO, NMO-1, NMO-2 And NMO-3 samples determined by ICP-OES (regard M=1).

Material	method	Electrochemical performance	reference
$Na_{0.44}MnO_2$	PVP-assisted gel combustion	0.1C (122mAh g^{-1}) 82.9%(700th at 10C)	[20]
$Na_{0.44}MnO_{1.93}F_{0.07}$	an oxalate precursor	5C (102mAh g^{-1}) 79% (400th at 5C)	[27]
$Na_{0.44}Mn_{0.98}Zr_{0.02}O_2$	an oxalate precursor	5C(100mAh g-1) 80%(1000th at 5C)	[S1]
$Na_{0.44}Mn_{0.95}Mg_{0.05}O_2$	solid-state reaction	30C(60mAh g-1) 72%(800th at 5C)	[S2]
$Na_{0.44}Mn_{0.9925}Co_{0.0075}O_2$	solid-state reaction	10C (93mAh g^{-1}) 85.2% (500th at 10C)	[29]
$Na_{0.44}MnO_2@In_2O_3$	solid-state reaction	10C(63.6mAh g-1) 86.7%(400th at 1C)	[S3]
$Na_{0.44}MnO_2@Al_2O_3$	solid-state reaction	8C(97.1mAh g-1) 96%(200th at 0.2C）	[S4]
$Na_{0.44}MnO_2$	electrospin and anneal	10C(69.5mAh g-1) 47%(150th at 1C)	[S5]
$Na_{0.44}MnO_2$	Microemulsion	8.3C(103mAh g-1) 88%(20th at 8.3C)	[S6]
$Na_{0.44}Mn_{0.97}(AlTiCo)_{0.01}O_2$	solid-state reaction	20C(80mAh g-1) 80%(2000th at 10C)	This work

Table S8: The electrochemical characteristics of several T-type $Na_{0.44}MnO_2$ cathode materials were compared.

REFERENCES

1. W. J. Shi, Y. M. Zheng, X. M. Meng, S. B. Liu, S. D. Xu, L. Chen, X. M. Wang and D. Zhang, Designing Sodium Manganese Oxide with 4 d-Cation Zr Doping as a High-Rate-Performance Cathode for Sodium-Ion Batteries, *ChemElectroChem*, 2020, **7**, 2545-2552.
2. X. L. Li, J. Bao, Y. F. Li, D. Chen, C. Ma, Q. Q. Qiu, X. Y. Yue, Q. C. Wang and Y. N. Zhou, Boosting Reversibility of Mn-Based Tunnel-Structured Cathode Materials for Sodium-Ion Batteries by Magnesium Substitution, *Adv. Sci. (Weinh)*, 2021, **8**, 2004448.
3. W. Liu, Q. Ren, M. Yang, L. Liu, Y. Zhang, D. Su, J. Wen, Q. Wang, X. Wang and Y. Feng, $Na_{0.44}MnO_2$ coated with In2O3 as a high-voltage cathode for sodium-ion batteries, *J. Alloy. Compd.*, 2022, **896**.
4. Y. Zhang, L. Liu, S. Jamil, J. Xie, W. Liu, J. Xia, S. Nie and X. Wang, Al_2O_3 coated $Na_{0.44}MnO_2$ as high-voltage cathode for sodium ion batteries, *Appl. Surf. Sci.*, 2019, **494**, 1156-1165.
5. B. Fu, X. Zhou and Y. Wang, High-rate performance electrospun Na0.44MnO2 nanofibers as cathode material for sodium-ion batteries, *J. Power Sources*, 2016, **310**, 102-108.
6. E. Hosono, T. Saito, J. Hoshino, M. Okubo, Y. Saito, D. Nishio-Hamane, T. Kudo and H. Zhou, High power Na-ion rechargeable battery with single-crystalline $Na_{0.44}MnO_2$ nanowire electrode, *J. Power Sources*, 2012, **217**, 43-46.